J Mater Sci (2006) 41:4928–4936
DOI 10.1007/s10853-006-0332-0

Interactions between nitrites and Fe(II)-containing phases during corrosion of iron in concrete-simulating electrolytes

L. Dhouibi · Ph. Refait · E. Triki · J. -M. R. Génin

Received: 5 March 2004 / Accepted: 15 September 2005 / Published online: 27 May 2006

Abstract The influence of sodium nitrite on the corrosion processes of iron in solutions simulating polluted concrete was investigated by means of electrochemical methods, such us potentiodynamic, galvanostatic and impedance spectroscopy tests, coupled with analyses of the corrosion layers by Mössbauer spectroscopy. NO_2^- ions are anodic inhibitors and provoked consequently an important increase of the corrosion potential. The polarisation curves show that NO_2^- ions increase the pitting potential value. The size of electrochemical impedance spectra obtained at the OCP increases with the concentration of nitrite, which confirms the decrease of the corrosion rate. Galvanostatic experiments allowed us to provoke active corrosion even in presence of NO_2^-. When nitrite ions are not present, the corrosion products mainly consist of iron (II) compounds, $FeCO_3$ or $Fe(OH)_2$ depending on the pH, and iron(II)–iron (III) compounds, i.e. green rusts (GRs). The main effect of nitrite ions was to accelerate the oxidation of GRs into FeOOH phases, confirming their oxidizing role. While immersed for long periods in the nitrite containing solutions, the α-iron foils do not present any single trace of corrosion.

L. Dhouibi (✉) · E. Triki
U. R. Corrosion et Protection des Métalliques, Ecole Nationale d'Ingénieurs de Tunis, BP 37, Le Belvédère, 1002 Tunis, Tunisia
e-mail: dhouibiala@yahoo.fr

Ph. Refait
Laboratoire d'Etudes des Matériaux en Milieux Agressifs, EA 3167 , Université de La Rochelle, Bâtiment Marie Curie, Avenue Michel Crépeau, F-17042 La Rochelle cedex 01, France

J. -M. R. Génin
Laboratoire de Chimie Physique et Microbiologie pour l'Environnement, UMR 7564 CNRS-Université Henri Poincaré-Nancy 1, Equipe Microbiologie et Physique, and Département Matériaux et Structures, ESSTIN, 405 rue de Vandoeuvre, F-54600 NancyNancy, France

Introduction

Sound concrete corresponds to an environment favouring the passivation of steel reinforcement and its subsequent protection against corrosion and degradation. However, the pollution of concrete by aggressive species such as chloride and carbon dioxide leads to a decrease of the pH and a breakdown of the passive film. It results in the corrosion of the steel reinforcing bars (rebars) and, in the long term, in the deterioration of the concrete. Carbonated and chloride polluted concrete corresponds mainly to basic aqueous media with large concentrations in both chloride and carbonate anions. Iron (II) and iron (III) salts as well as green rusts (GRs), that is iron (II)–iron (III) hydroxy-salts, constitute some examples of important corrosion products possibly involved in the corrosion of steel rebars in concrete. According to previous works devoted to the chloride and carbonate forms of GRs [1–4], concrete would be one of the most favourable media for their appearance. A first study [5] was then devoted to the early stages of the corrosion of steel in electrolytes simulating concrete and to the ability of phosphate to inhibit this degradation. It confirmed that GRs are the main products of the initial stages of the corrosion process and demonstrated the efficiency of PO_4^{3-} as an inhibitor.

Since calcium nitrite $Ca(NO_2)_2$ is an inhibitor commonly used in concrete today, the accurate knowledge of the possible interactions between GRs and NO_2^- ions is a clue

for the understanding and optimisation of this inhibition. This work was then focused on the mechanisms of the inhibition of the corrosion of iron in concrete pore waters based on saturated $Ca(OH)_2$ solution added with chloride, carbonate species and nitrite. A previous work has shown that electrochemical results in saturated calcium hydroxide were similar to those obtained in concrete [6]. The present study was performed by means of electrochemical methods, such as galvanostatic, polarisation curves, and impedance spectroscopy experiments, coupled with analyses of the corrosion products by transmission Mössbauer spectroscopy (TMS). The role of nitrite will be compared with that of phosphate.

Experimental

Electrochemical tests

Three types of solutions were used for simulating the conditions met in various types of concrete. Their molar composition and pH are given in Table 1. Solution S_1 is intended to simulate a fresh concrete containing some chloride ions; solutions S_2 and S_3 simulate carbonated concrete containing Cl^- ions. $NaNO_2$ was used to provide nitrite ions. The amount added was related to the Cl^- concentration and expressed with the ratio $R = [NO_2^-]/[Cl^-]$. Three values were considered: $R = 0$, i.e. the reference solution without nitrite, $R = 0.4$ and $R = 1$.

α-Iron foils of 50 μm thick, provided by Goodfellow® were used to prepare 34 mm diameter (*i.e.* a surface of 9 cm^2) working electrodes. These electrodes were cleaned with acetone and distilled water and dried in warm air. Their sides were coated with an electric insulator while a copper wire was welded at an extremity to provide the connection to the electrical circuit needed for electrochemical testing. It was finally set in a three-electrode cell containing 250 ml of solution, with a saturated calomel electrode for reference and a platinum wire as counter-electrode. The solution was slightly agitated and maintained at a temperature of 25 ± 1 °C during tests. A Radiometer-Tacussel® PGP201 potentiostat–galvanostat monitored by the Voltamaster-1® software was used for galvanostatic and polarisation curves measurements. In each case, the corrosion potential E_{cor} was measured and plotted against time during 1 h before experiments. For galvanostatic test, a current density of 0.5 mA cm^{-2} was then maintained for 5 h to rapidly induce the formation of a sufficient amount of corrosion products. Polarisation curves were drawn from the corrosion potential up to an anodic current of 200 μA cm^{-2} at a scanning rate of 25 mV min^{-1}, followed by a similar scan in the reverse direction down to –1255 mV_{SHE}. Impedance spectroscopy was performed within the same cell. The equipment consisted of a potentiostat (Solartron SI 1286®), an analyser of transfer function (Solartron FRA SI 1250®), a filter (Kemo VBF8®) and a PC computer with FRACOM software for plotting impedance by controlling the analyser of transfer function and a SIMPLEX software for modelling experimental data by an ''Equivalent Electric Circuit''. Plotting on the same graph the experimental and calculated Nyquist diagrams checked the validity of the calculated results. Steel was polarised at ±10 mV around its zero-current potential. Frequency was ranging between 65 kHz and 10 mHz, with 5 frequency values per decade.

It can be noticed that for reproducibility, each electrochemical test was repeated three times. The experimental error did not exceed 10%.

Analyses of the solid phases

The products obtained after galvanostatic tests were scraped from α-iron foils and analysed by TMS at room temperature. In order to avoid any subsequent oxidation, these products were immediately set in the sample holder and kept under inert helium atmosphere during spectrum accumulation. The Mössbauer apparatus consists of a conventional constant acceleration spectrometer calibrated with a 25 μm α-iron foil at room temperature.

Results

Electrochemical tests

Figure 1 shows the behaviour of the corrosion potential E_{cor} with time for α-iron dipped in S_1, S_2 and S_3 solutions with ratio $R = [NO_2^-]/[Cl^-] = 0$, 0.4 and 1. It appears that the stabilisation (±30 mV) occurred rapidly, after approximately half an hour. In the absence of nitrite ($R = 0$), the

Table 1 Composition and pH of the solutions considered in order to simulate concrete media

Solution	Concentrations (mol L^{-1})				pH for $R = [NO_2^-]/[Cl^-]$		
	$Ca(OH)_2$	NaCl	$NaHCO_3$	Na_2CO_3	$R = 0$	$R = 0.4$	$R = 1$
S_1	Saturated	0.5	–	–	12.1	12.1	12.1
S_2	–	0.5	0.6	–	8.2	8.1	8.1
S_3	–	0.5	0.3	0.15	9.4	9.3	9.3

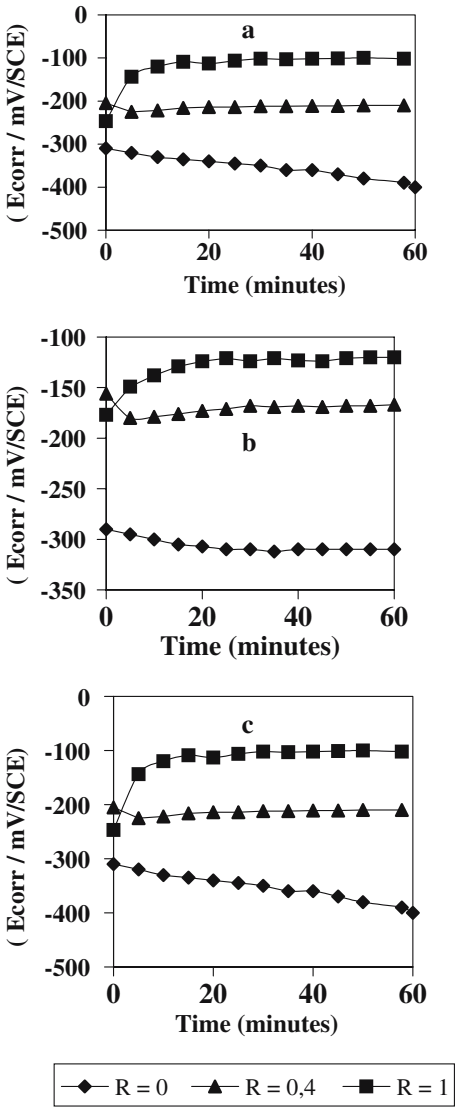

Fig. 1 Influence of nitrite on the evolution of the corrosion potential E_{cor} versus time in (**a**) solution S_1, (**b**) solution S_2 and (**c**) solution S_3. $R = [Cl^-]/[NO_2^-]$

potential decreases with time, which denotes an active behaviour due to chloride ions. Moreover, the measured values decrease when the pH increases. In the presence of nitrite, the potential stabilises at more noble values. The increase in E_{cor}, e.g. about 300 mV for $R = 1$, suggests a predominant anodic inhibition.

Figure 2 gives the electrochemical impedance diagrams at zero current potential in the Nyquist's plot for α-iron dipped in S_1, S_2 and S_3 solutions with ratio $R = [NO_2^-]/[Cl^-] = 0$, 0.4 and 1. In all cases, they are made of a capacitive loop, which is slightly centred off the real axis. When adding nitrite ions, the outlook of the impedance diagrams is not modified. A simple Randles equivalent circuit $R_e(R_tC_{dl})$ (electric resistance, R_e, charge transfer resistance, R_t and double layer capacitance, C_{dl}) was used

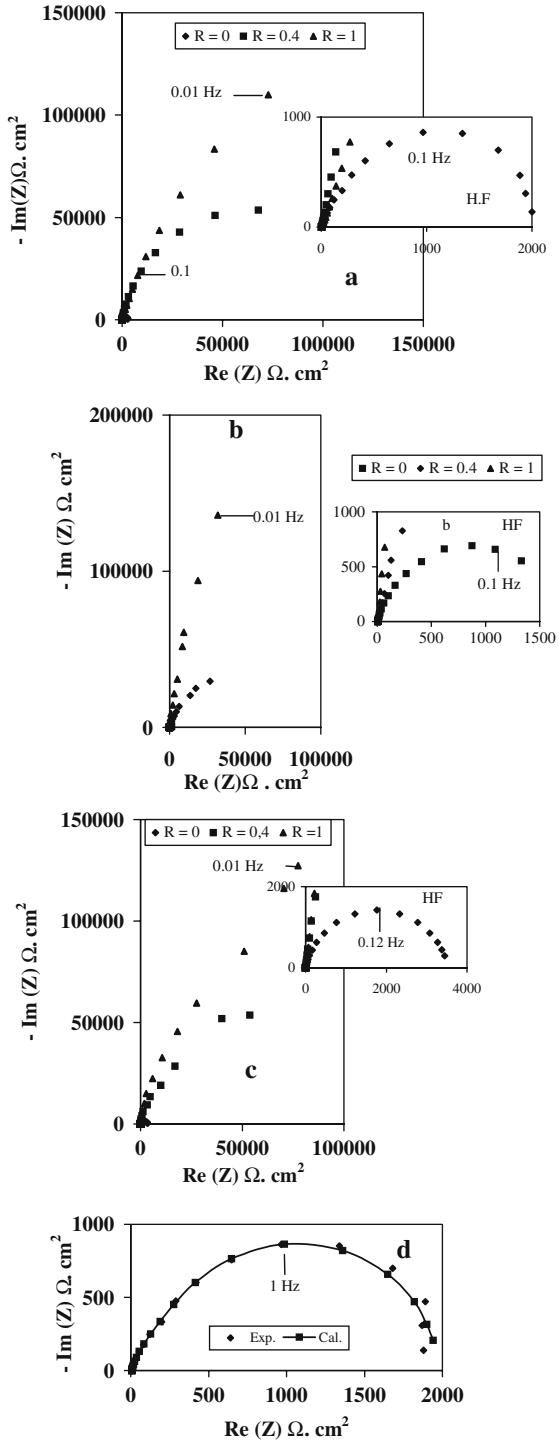

Fig. 2 Nyquist diagrams of α-iron in (**a**) solution S_1, (**b**) solution S_2 and (**c**) solution S_3, with or without nitrite added as an inhibitor. (**d**) Experimental and calculated EIS diagrams: example of α-iron in solution S1 at R = 0. $R = [Cl^-]/[NO_2^-]$

for fitting the EIS Nyquist plots. It must be noted that the best fit was obtained by introducing a symmetrical Cole–Cole distribution on the time constant. In all cases, a discrepancy, which was less than 5%, was observed between

experimental and calculated values of the impedance. Figure 2d shows the comparison between experimental and calculated typical EIS Nyquist plot. Thus, the electric model describes the interface and consequently the experimental diagrams can be used to determine the values of the various elements in the electric circuit. Table 2 gathers the values obtained in each case for these parameters. It appears that the electrolyte resistance R_e, which is in series with the other elements, decreases slightly with nitrite addition. The solution becomes more conducting but its nature does not change. The resistance R_t that corresponds to the diameter of the capacitive arc increases strongly with nitrite content The interface capacity C_{dl} is close to or higher than the double layer capacitance. According to some works [7], the increase of the C_{dl} capacity can be explained either by an increased iron surface caused by the corrosion process or by the higher concentration of charges in the diffuse double layer. Generally speaking, the resistance R_t increases and the capacitance C_{dl} decreases with inhibitor addition. Thus, the inhibitor diminishes drastically the metal dissolution rate and consequently the corrosion intensity. The interface response can be related to a charge transfer process.

As pitting corrosion is important in chloride environment, the pitting potential E_p and the repassivation potential E_{rep} are of interest. It is to be noticed that E_p is the potential where a first pit appears, when no initial pit exists before the potential scanning starts. E_{rep} is the potential where the reverse scan intersects with the forward scan. It corresponds to the potential value that must be applied in order to repassivate the well-grown pits where the electrolyte has changed towards more severe conditions. In such pits, the pH decreased and the chloride concentration increased. In the absence of pitting, forward and reverse scans coincide. Figure 3 displays a typical example of the polarisation curves for α-iron dipped in S_1 solution with ratio $R = [NO_2^-]/[Cl^-] = 0$, 0.4, 1 and Table 3 gathers these specific potentials for all the studied systems. It appears that E_p and E_{rep} shift towards more noble values whereas the passivation plateau increases with the inhibitor concentration. Therefore, nitrite ions increase the resistance of iron to pitting corrosion in solutions simulating polluted concrete.

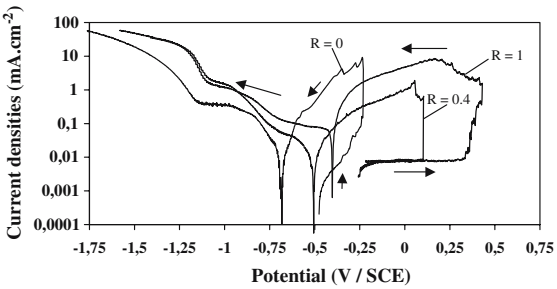

Fig. 3 Polarisation curves of α-iron dipped is solution S_1 at various $R = [Cl^-]/[NO_2^-]$ values

Figure 4 displays the galvanostatic curves. In each case, the evolution is typical of an active system. The potential drops rapidly then it stabilises at potential values approximately 200 mV larger than the corrosion potential. In each case, the metal surface is covered with corrosion products at the end of the experiment.

Analyses of the corrosion products

TMS analyses of the products obtained without NO_2^- ($R = 0$) with or without phosphate [5]

TMS analysis at room temperature of the corrosion product formed after galvanostatic experiments on the iron foil in the solution S_2 free of nitrite ($R = 0$) is presented in Fig. 5. This product did not adhere to the metal and was easily removed from the surface. Its spectrum is mainly composed of two ferrous quadrupole doublets, D_1 and FC, characterised by large isomer shifts δ and quadrupole splittings Δ (Table 4), and one ferric doublet D_3 that corresponds to smaller δ and Δ values. The ferrous doublet D_1 and the ferric doublet D_3 are attributed to a green rust compound. The Δ value of the ferrous component, *i.e.* 2.35 mm s^{-1}, was already observed for such compounds at room temperature [4]. Moreover, the D_1/D_3 intensity ratio, that is the Fe(II)/Fe(III) ratio, is about 3, a value often met in GRs [1, 4, 8–10]. Since CO_3^{2-} ions are preferred over any

Table 2 Characteristic parameters of the α-iron-solution-inhibitor interface

Solution	S_1			S_2			S_3		
R	0	0.4	1	0	0.4	1	0	0.4	1
R_e (Ω cm^2)	5.6	4.4	3.4	4.3	4	3.5	3.7	3.2	3.1
C_{dl} (μF cm^{-2})	82	72	50	420	198	150	360	75	98
α	0.85	0.88	0.81	0.88	0.84	0.89	0.81	0.92	0.90
R_t (kΩ cm^2)	2	100	134	1.76	89	120	2.75	98	138
F (Hz)	0.98	0.021	0.025	0.22	9.10^{-3}	9.10^{-3}	0.16	0.022	0.01

$R = [NO_2^-]/[Cl^-]$

Table 3 Pitting potential E_p and repassivation potential E_{rep} at R = $[NO_2^-]/[Cl^-]$ = 0, 0.4 and 1 in S_1, S_2 and S_3 solutions

Solution	S_1			S_2			S_3		
R	0	0.4	1	0	0.4	1	0	0.4	1
E_p	–240	120	360	–155	150	280	–190	295	380
E_{rep}	–680	–500	–400	–395	–205	–173	–385	–215	–185

Values are given in mV with respect to the saturated calomel electrode. $E \pm 30$ mV_{SCE}

other anion, and especially monovalent ones [11, 12], the GR observed in solution S_2 is necessarily $GR(CO_3^{2-})$. For instance, in $NaHCO_3$ + NaCl solutions with $[Cl^-]/[HCO_3^-]$ ratio of 40, the corrosion process was demonstrated to produce $GR(CO_3^{2-})$ [3]. Doublet *FC* is characterised by a smaller Δ value of 1.81 mm s^{-1}. Such a value at room temperature is characteristic of the iron (II) carbonate $FeCO_3$ [13].

The analysis related to solution S_3 (not represented) confirmed the presence of both $GR(CO_3^{2-})$ and $FeCO_3$, related to solution S_1, revealed the presence of $GR(Cl^-)$ and $Fe(OH)_2$.

Similar experiments were performed in the presence of phosphate with ratios $[Cl^-]/[PO_4^{3-}]$ equal to 0.4 or 1 [5]. The TMS analysis at room temperature of a typical corrosion product formed after galvanostatic experiments is presented in Fig. 6 and the corresponding data in Table 4. This product, obtained in the solution S_2 for $[Cl^-]/[PO_4^{3-}]$ equal to 1, was found in small amounts localised around a few pits on the metal and adhered to the surface. It was then scraped from the iron foil, which explains the presence of the sextet due to α-Fe. The main difference between this spectrum and the previous one (Fig. 5) is the presence of an important Fe(III) doublet *F*. Additional analyses revealed that it corresponded to ferrihydrite, the most poorly ordered form of Fe(III) oxyhydroxides. $GR(CO_3^{2-})$, identified by its Fe(II) doublet D_1, is still present, indicating that the corrosion process is the same. The average oxidation number of iron increased indicating

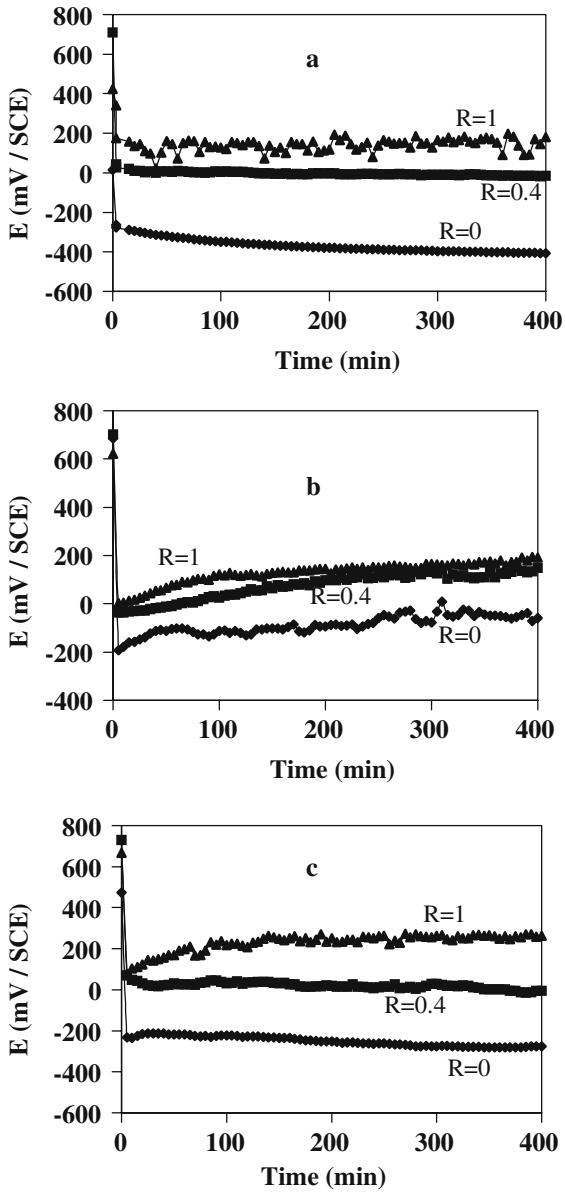

Fig. 4 Potential versus time curves during galvanostatically induced corrosion of α-iron dipped in various solutions at various $R = [Cl^-]/[NO_2^-]$ values. (**a**) Solution S_1, (**b**) solution S_2 and (**c**) solution S_3

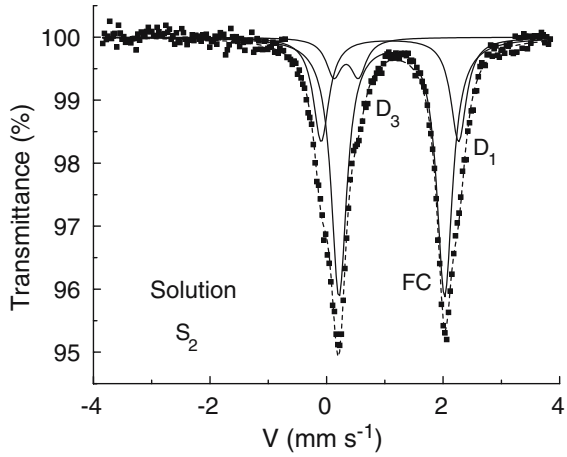

Fig. 5 Mössbauer spectrum measured at room temperature of the corrosion product obtained after galvanostatic experiment in solution S_2 without any inhibitor ($R = 0$)

Table 4 Mössbauer hyperfine parameters at room temperature of the corrosion products obtained after galvanostatic experiments

Doublet	Solution S_2 at R = 0 (Fig. 6)				Solution S_3 with PO_4^{3-} (Fig. 7)			
	δ	Δ	H	RA	δ	Δ	H	RA
D_1	1.21	2.35	–	26	1.24	2.44	–	19
FC	1.24	1.81	–	65	–	–	–	–
D_3	0.46	0.42	–	9	–	–	–	–
F	–	–	–	–	0.52	0.69	–	66
a-Fe	–	–	–	–	0	0	331	15
Doublet	Solution S_1 with NO_2^- at R = 1 (Fig. 7a)				Solution S_3 with NO_2^- at R = 0.4 (Fig. 7b)			
	δ	Δ	H	RA	δ	Δ	H	RA
D_1	–	–	–	–	1.2	2.4	–	2
F_1	0.35	0.56	–	55	0.37	0.62	–	62
F_2	0.35	0.96	–	33	0.37	1.01	–	30
a-Fe	0	0	331	12	0	0	331	6

δ = isomer shift with respect to α-iron in mm s^{-1}; Δ = quadrupole splitting in mm s^{-1} ; H = hyperfine field in kOe; RA = relative abundance in %. Full widths at half maximum were constrained to be equal for each Lorentzian-shape line

that the extent of the oxidation reaction is larger. This is mainly due to the fact that the corrosion was localised on a few pits, implying a larger current density, which is a more rapid oxidation process. The presence of ferrihydrite as the final product of this oxidation may result from a specific action of phosphate. It was actually demonstrated that orthophosphate could induce the transformation of GR(CO_3^{2-}) into ferrihydrite [14].

TMS analyses of the products obtained for R > 0

The corrosion products obtained galvanostatically in the presence of NO_2^- ions adhered to the iron surface. They were scraped from the metal, revealing that a lot of pits have formed under the rust layer. Two typical Mössbauer spectra of these products, namely that related to solution S_1 with R = 1 and that related to solution S_3 with R = 0.4 are presented in Fig. 7. Other spectra (not represented) are similar whatever the solutions considered and whatever the value of R. They all consist of the spectral component of α-Fe accompanied by Fe(III) quadrupole doublets F_1 and F_2, and in some cases, by a minor Fe(II) doublet D_1. The hyperfine parameters of D_1 (Table 4) are typical of Fe(II) in GRs. F_1 is a typical doublet of FeOOH phases. It could be attributed whether to γ-FeOOH lepidocrocite [15], to poorly crystallised goethite, which gives rise to a so-called ''superparamagnetic'' spectrum at room temperature [16], or ferrihydrite [17]. Each of these compounds is a by-product of the oxidation of GRs [1–4, 14]. F_2, with a large Δ value, is characteristic of poorly crystallised and poorly ordered FeOOH phases.

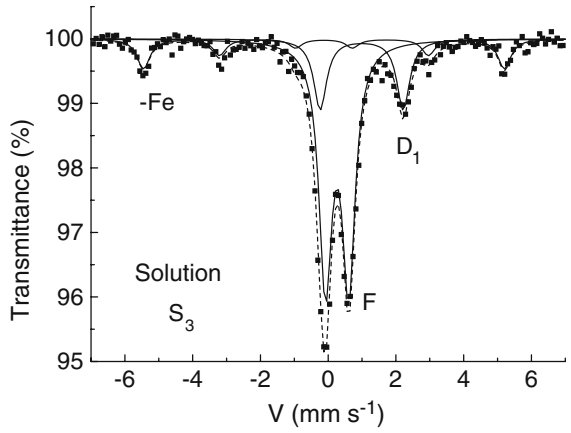

Fig. 6 Mössbauer spectrum measured at room temperature of the corrosion product obtained after a galvanostatic experiment in solution S_3 with PO_4^{3-} as an inhibitor

The TMS spectra of the corrosion products resulting of the action of nitrite can be compared to the spectrum of Fig. 6 that presents the analysis of the corrosion products obtained in the same conditions with phosphate instead. The trend is similar, the Fe(III) compounds are in both cases favoured due to the localisation of the process. But the effects are quantitatively different. With NO_2^-, only traces of GR(CO_3^{2-}) are present. With PO_4^{3-}, GR(CO_3^{2-}) is still present in non-negligible proportion. Moreover, when only a few pits were observed on the steel surface immersed in PO_4^{3-} containing electrolytes, a lot of pits and a greater amount of corrosion products were seen on surfaces immersed in NO_2^- containing electrolytes. The corrosion is more localised when phosphates are present but, in contrast, the corrosion products have a larger average oxidation number when nitrites are present.

Finally, it must be noted that some α-iron foils were also immersed at open circuit potential for 1 week in the concrete-simulating solutions with NO_2^- at $R = 1$. They did not show any corrosion, confirming the inhibiting effect of nitrite ions.

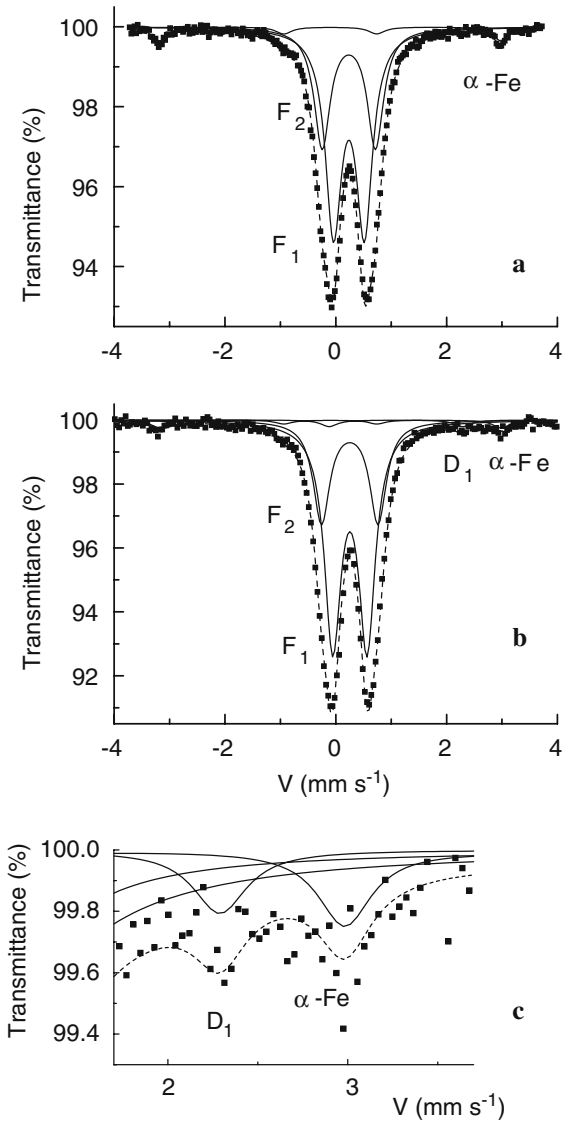

Fig. 7 Mössbauer spectra measured at room temperature of the corrosion products obtained after galvanostatic experiments in solutions containing NO_2^- as an inhibitor. (**a**) Solution S_1 with $R = [Cl^-]/[NO_2^-] = 1$, (**b**) solution S_3 with $R = [Cl^-]/[NO_2^-] = 0.4$, (**c**) enlargement of the previous spectrum in the region showing one peak of doublet D_1

Discussion

Mechanisms of the corrosion of α-iron in concrete simulating solutions

Five hours of galvanostatically induced corrosion led to the formation of iron (II) and iron (II)–iron (III) compounds. In any case, the corrosion of iron in concrete-simulating solutions involved GR compounds. In the presence of oxygen, GRs are unstable and oxidised into the usual components of rust, that is mainly γ-FeOOH, α-FeOOH, Fe_3O_4 [1–4], or even β-FeOOH [18], depending on various parameters such as temperature, dissolved oxygen concentration, pH, etc. Besides GRs, various iron (II) compounds were observed, namely $Fe(OH)_2$ and $FeCO_3$. $Fe(OH)_2$ would appear only at lower carbonate concentrations and/or higher pH values, as it is the case for solution S_1. This compound is known to be a precursor of green rust iron (II)–iron (III) hydroxy-compounds, such as $GR(Cl^-)$ [1] or $GR(CO_3^{2-})$ [2]. According to the Pourbaix diagram previously drawn for iron in chloride-containing solution with $[Cl^-]$ close to 1 mol l^{-1} [4], $GR(Cl^-)$ could form in a range of pH from 7.8 to 12.8. The identification of $GR(Cl^-)$ as a corrosion product of iron in solution S_1 with a pH value of 12.4 is then in full agreement with the behaviour predicted by the diagram.

Finally, even though $GR(CO_3^{2-})$ is metastable with respect to $FeCO_3$ at most pH values and carbonate concentrations, the formation of $GR(CO_3^{2-})$ from iron was reported to occur easily [3], and, actually, this compound was first observed as the corrosion product of cast iron water pipes [19]. In general, the formation of this GR should be favoured instead of $FeCO_3$ when the pH increases or when the concentration of carbonate species decreases.

Influence of nitrite ions on the corrosion processes

The absence of any detectable corrosion process during the immersion of the α-iron foils in the various nitrite containing solutions at $R = 1$ testifies to the effectiveness of the inhibition. This inhibiting effect allows the passive film of iron oxide, more likely γ-Fe_2O_3 [20–22], to remain.

The results obtained by impedance spectroscopy show that at OCP, the Nyquist plots are formed of one capacitive loop. Its diameter increases with the inhibitor content and the corresponding capacitances decrease. This confirms that the nitrite ions do not form an inhibitor film at the metallic surface.

The galvanostatic experiments allowed us to induce pitting corrosion in the presence of NO_2^-. Since traces of a GR compound were seen on some of the samples, it can be assumed that the corrosion process is similar to what happens without NO_2^-, that is, schematically:

$$Fe \xrightarrow{(1)} Fe_{aq}^{2+} \xrightarrow{(2)} FeCO_3 \text{ and } GR(CO_3^{2-}) \xrightarrow{(3)} FeOOH,$$

in carbonated media, and:

$$Fe \xrightarrow{(1)} Fe_{aq}^{2+} \xrightarrow{(2)} Fe(OH)_2 \text{ and } GR(Cl^-) \xrightarrow{(3)} FeOOH,$$ in chlorinated media.

where (1) is dissolution of iron; (2) is precipitation of Fe(II) bearing phases and (3) oxidation of these phases into FeOOH.

However, the presence of NO_2^- increases the kinetics of oxidation of the GRs and other Fe(II) compounds, leading

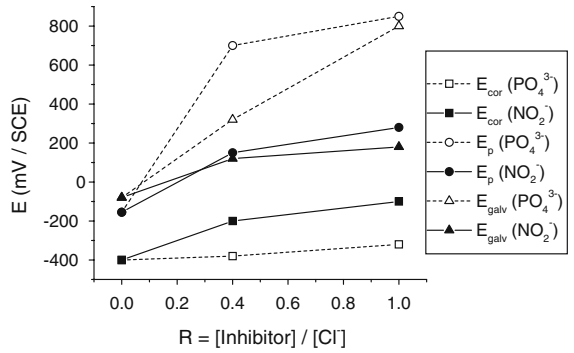

Fig. 8 Evolutions of the corrosion potential E_{cor}, the pitting potential E_p and the potential measured during galvanostatic experiments E_{galv} with the inhibitor concentration. Comparison between the values obtained with PO_4^{3-} as an inhibitor [5] and the values obtained here using NO_2^- as an inhibitor

to the rapid formation of FeOOH phases. This can be related to the reactivity of GRs towards NO_2^- ions [23]. In particular, the oxidising effect of NO_2^- is evidenced by comparing the results obtained here to those obtained previously with PO_4^{3-} as an inhibitor [5]. In Fig. 8 the E_{cor} and E_p values are reported versus the ratio R = [inhibitor]/[Cl^-]. It can be seen that phosphate produces a considerable increase of the pitting potential, which testifies to the favourable influence of this inhibitor upon the stability of the passive film. In contrast, it has almost no influence on the corrosion potential E_{cor}, as PO_4^{3-} is not an oxidising inhibitor. The slight increase of E_{cor} may reflect an increase of the passive film thickness.

The effects of NO_2^- on those potential values are quite different. The increase of E_p is significant but in no way comparable to that produced by phosphate. E_{cor} is also increased and the difference E_{cor}–E_p is almost constant. This indicates clearly that nitrite acts as an anodic inhibitor, favouring the oxidation of Fe(II)-containing solids and thus preserving the Fe(III)-based passive film. Note finally that the potential corresponding to the galvanostatic experiments E_{galv} is close to the E_p value, except in one case (R = 0.4 with PO_4^{3-}) where it is larger.

The oxidising action of nitrite ions is also revealed by the Mössbauer analyses. Without inhibitors, uniform corrosion occurred during galvanostatic polarisation and $Fe(OH)_2$, $FeCO_3$ and GRs were formed. The effect of phosphate was to localised the corrosion in a few pits, where a mixture of GRs and FeOOH phases (mainly ferrihydrite) were formed. The effect of nitrite was to accelerate the oxidation, leading to FeOOH phases with, in some cases, traces of GRs. Therefore, the effects of NO_2^- can be summarised as follows:

– When pitting corrosion occurs, NO_2^- facilitate the transformation of GRs and other Fe(II) solids into FeOOH phases.

– In the absence of stable pitting corrosion processes, NO_2^- may promote repassivation by transforming Fe(II) containing species into the spinel oxides Fe_3O_4 and γ-Fe_2O_3 that constitute the passive film. This is similar to a previous model proposed by Berke et al. [23] where the repassivation is attributed to the action of NO_2^- upon Fe^{2+}_{aq}:

$$2Fe^{2+} + 2OH^- + 2NO_2^- \rightarrow 2NO + Fe_2O_3 + H_2O$$

The action of NO_2^- may be generalised to most of the reactive Fe(II) containing corrosion products.

Conclusions

Electrochemical tests and Mössbauer analyses of the corrosion products were coupled successfully to study the behaviour of α-iron in solutions simulating concrete, with and without NO_2^- as an inhibitor. It was deduced that:

- Nitrite ions are anodic inhibitors that increase the resistance to pitting attack and decrease the corrosion rate when chlorides are present. It can be guaranteed for a large nitrite concentration, matching that of chloride ions, whereas some pitting may occur, should this concentration be too small.
- The early stages of the corrosion processes involve GR compounds and other Fe(II) containing phases, namely $Fe(OH)_2$ and $FeCO_3$. The oxidising action of nitrite favours and accelerates the oxidation of Fe^{2+}_{aq} and Fe(II) containing phases, which facilitates repassivation and improves the corrosion resistance.

Acknowledgements The authors would like to thank Dr. Mustapha Abdelmoula for his help in accomplishing the Mössbauer experiments. This study was made possible by the DGRST-CNRS agreement between Tunisia and France and a grant to one of them (L. D.).

References

1. Refait Ph, Génin J-MR (1993) Corros Sci 33:797
2. Drissi SH, Refait Ph, Abdelmoula M, Génin J-MR (1995) Corros Sci 37:2025
3. Abdelmoula M, Refait Ph, Drissi SH, Mihé J-P, Génin J-MR (1996) Corros Sci 38:623
4. Refait Ph, Abdelmoula M, Génin J-MR (1998) Corros Sci 40:1547
5. Dhouibi L, Refait Ph, Abdelmoula M, Triki E, Génin J-MR (2002) Corrosion 58:467
6. Hachani L, Carpio J, Fiaud C, Raharinaivo A, Triki E (1992) Cement Concrete Res 22:56
7. Pruckner F (2001) Thesis, Faculty Nat Sci Math. Vienna
8. Detournay J, Dérie R, Ghodsi M (1976) Z anorg allg Chem 427:265

9. Schwertmann U, Fechter H (1994) Clay Miner 29:87
10. Simon L, Génin J-MR, Refait Ph (1997) Corros Sci 39:1673
11. Mendiboure A, Schöllhorn R (1986) Rev Chim Min 23:819
12. Refait Ph, Drissi SH, Pytkiewicz J, Génin JM (1997) Corros Sci 39:1699
13. Forester DW, Koon NC (1969) J Appl Phys 40:1316
14. Benali O, Abdelmoula M, Refait Ph, Génin J-MR (2001) Geochim et Cosmochim Acta 65:1715
15. Rossiter MJ, Hodgson AEM (1965) J Inorg Nucl Chem 27:63
16. Morup S, Madsen MB, Franck J, Villadsen J, Koch CJW (1983) J Magn Magn Mater 40:163
17. Murad E, Schwertmann U (1980) Amer Min 65:1044
18. Refait Ph, Génin J-MR (1997) Corros Sci 39:539
19. Stampfl PP (1969) Corros Sci 9:185
20. Pryor MJ, Cohen M (1953) J Electrochem Soc 100:203
21. Mayne JEO, Menter JW (1954) J Chem Soc 103
22. Szklarska-Smialowska Z, Staehle RW, (1974) J Electrochem Soc 121:1393
23. Berke N, Hicks MC (1997) Conf. on understanding corrosion mechanisms in concrete, Cambridge, Massachusetts, USA
24. Hansen HCB, Borggaard OK, Sorensen J (1994) Geochim Cosmochim Acta 58:2599